

Dynamical charge and spin currents in graphene and possible Cooper pair formation

K. Morawetz^{1,2,3}

¹*Münster University of Applied Sciences, Stegerwaldstrasse 39, 48565 Steinfurt, Germany*

²*International Institute of Physics (IIP) Federal University of Rio Grande do Norte Av. Odilon Gomes de Lima 1722, 59078-400 Natal, Brazil and*

³*Max-Planck-Institute for the Physics of Complex Systems, 01187 Dresden, Germany*

Based on the quantum kinetic equations for systems with SU(2) symmetry, regularization-free density and spin currents are calculated in graphene realized as the infinite mass-limit of electrons with quadratic dispersion and a proper spin-orbit coupling. Correspondingly the currents possess no quasiparticle part but only anomalous parts. The intraband and interband conductivities are discussed with respect to magnetic fields and magnetic domain puddles. It is found that the magnetic field and meanfield of domains can be represented by an effective Zeeman field. For large Zeeman fields the dynamical conductivities become independent of the density and are universal in this sense. The different limits of vanishing density, relaxation, frequency, and Zeeman field are not interchangeable. The optical conductivity agrees well with the experimental values using screened impurity scattering and an effective Zeeman field. The universal value of Hall conductivity is shown to be modified due to the Zeeman field. The spin current reveals an anomaly since a quasiparticle part appears though it vanishes for particle currents. The density and spin response functions to an external electric field are calculated and the dielectric function is discussed with respect to collective excitations. A frequency and wave-vector range is identified where the dielectric function changes sign and the repulsive Coulomb potential becomes effectively attractive allowing Cooper pairing.

PACS numbers: 72.25.-b, 75.76.+j, 71.70.Ej, 85.75.Ss

I. INTRODUCTION

Graphene has been the topic of tremendous theoretical activity with many complete reviews published¹⁻³. The question is what one might find new besides these many excellent investigations. In order to provide a systematic approach allowing successively better approximation, one aim is to describe all transport properties and excitation properties with the help of a single theoretical method which will be here the quantum kinetic theory. Another goal is to explore new branches of excitations which might not be treated yet. Here it will be presented a quantum kinetic approach to these transport properties including magnetic fields and meanfields due to magnetic domains. The range of parameters is explored where the effective Coulomb interaction between the electrons in graphene might change the sign. This allows to pair the electrons as a necessary condition for superconductivity.

In graphene the chiral nature of the charge carriers leads to a minimal finite conductivity even with vanishing density of scatterers. If there are no charge carriers the field has to create first electron-hole pairs before it can be accelerated. Since the absolute value of the velocity is fixed, only the direction can change which provides an anomaly transport⁴. This remarkable feature of dissipation in an even ideal crystal is reached in various limiting procedures. The static limit and vanishing relaxation rate are not interchangeable as it was noted⁵. If one first take the static limit and then the collision free limit one obtains

$$\sigma_1 = g \frac{e^2}{2\pi^2\hbar} \quad (1)$$

while the opposite order provides

$$\sigma_2 = g \frac{e^2}{16\hbar} \quad (2)$$

which agrees within 1 – 2% with experiments⁶⁻⁸ taking into account the valley degeneracy $g = 4$. Sample-dependent fore-factors⁹ have been attributed to inhomogeneous charge distributions around the Dirac point¹⁰. Twice σ_2 is obtained if one takes the limit $\omega = \hbar/\tau$ ^{11,12}.

This different limiting values have raised many theoretical investigations³. Both results have been obtained by Kubo formula approaches depending on the order of limits performed. In¹³ the result σ_2 was obtained with the factor of 2 for bilayer graphene and the result for multilayer graphene was given in¹⁴. The density matrix approach¹⁵ discusses the parallels between steady states reached in graphene and the precession motion in spin-orbit coupled systems. The surface state of a topological insulator with the effective Hamiltonian $Dp^2 + \lambda\vec{\sigma} \cdot \vec{p}$ has been treated in¹⁶ where the limit $D \rightarrow \infty$ leads to the correct result. It is argued that the transition between both regimes is due to low and high density limits. We will use the limit of infinite mass to extract the specific results for graphene from results of the general transport theory for SU(2) systems¹⁷.

The tight binding approach in electric field⁴ provides essentially the correct expression σ_2 and discusses two theoretical classes leading to the wrong result σ_1 . Essentially there is no small parameter as the usual Ioffe rule $\hbar/\epsilon_F\tau$ and diagrammatic approaches miss probably important diagrams. The second class of treatments leading to σ_1 relies on the Landauer approach and takes the limiting value of finite width and length of the ribbon sample. This is performed by counting evanescent modes¹⁸.

There it was claimed that the appearance of the minimal conductivity is due to the topological property of the Berry phase and nature of evanescent waves and is not a signal of Zitterbewegung and chiral symmetry as suggested in^{19,20}

The influence of impurity and phonon scattering has been investigated in high electric fields²¹ within a balance equation approach. It is suggested that the electron-electron interaction or strains in the sample causes a symmetry breaking which was modeled by a complex parameter²² leading to σ_1 .

The expansion around the correct value $\sigma_2(1 + C\alpha_V)$ in terms of fine structure constant of graphene $\alpha_V = e^2/(4\pi\hbar v) \approx 2.2$ had raised a controversy. The two loop interaction correction was calculated in two ways, via density-density and current-current correlation functions with the help of dimensional regularization²³. In²⁴ it was claimed to have found the reason for the discrepancy in the first-order expansion by calculating a tight binding approach before reduction to mass-less Dirac particles. The different results are dependent on the used regularization schemes. The sharp momentum cut-off used by²⁵ leading to $C = 25/12 - \pi/2$ had been criticized by Mishenko²⁶ obtaining $C = 19/12 - \pi/2$ due to soft cut-off. This has been supported by²⁷ which states the importance of charge conservation at all stages of approximation and completion of Ward identity. The reason for the discrepancy with the sharp cut-off has been traced in²⁸ to be due breaking of transversality of the polarization tensor which is a consequence of the spatial O(2) symmetry. The soft cut-off result has been reproduced there with a regularization-independent framework discussing Coulomb corrections²⁹. A first-order interaction correction to the polarization function and dielectric function was treated in³⁰ and compared with other renormalization approaches. We will present a scheme which is free of any regularization.

Recently there has been tremendous effort to modify the graphene sheets in order to create a gap which is necessary for optical applications^{1,31}. Nanoribbons^{32,33}, twisted bilayers³⁴, disordered graphene³⁵, or nanofluids^{36,37} are some possibilities. In this context the suggestion was made that on the surface charge puddles appear³⁸⁻⁴⁰. We model such domains assuming that this local magnetic fields are randomly distributed on different sites within an angle θ_l from the \vec{e}_z direction. The directional average⁴¹ leads then to

$$\begin{aligned} \sum_p \overline{f\vec{V}} &= |V| \frac{\sin \theta_l}{\theta_l} \vec{e}_z n = \vec{V}(q) n(q) \\ \sum_p \overline{g\vec{V}} &= |V| \frac{\sin \theta_l}{\theta_l} \vec{e}_z s = \vec{V}(q) s(q) \end{aligned} \quad (3)$$

where the density and polarization density are given by

$$\sum_p f(\vec{p}, \vec{q}, t) = n(\vec{q}, t), \quad \sum_p \vec{g}(\vec{p}, \vec{q}, t) = \vec{s}(\vec{q}, t) \quad (4)$$

and $\sum_p = \int d^D p / (2\pi\hbar)^D$ for D dimensions. The magnetization density becomes $\vec{M}(\vec{x}) = g\mu_B \vec{s}(\vec{x})$.

The angle θ_l in (3) allows us to describe different models. A completely random local magnetic field $\theta_l = \pi$ is used for magnetic impurities in a paramagnetic spacer layer and in a ferromagnetic layer one uses $\theta_l = \pi/4$. The latter one describes the randomly distributed orientation against the host magnet⁴¹. Therefore the same impurity potential appears as magnetic impurities. We will see that it adds to the Zeeman field and we will call it effective Zeeman field during this paper.

The outline of the paper is as follows. First we sketch shortly the quantum kinetic approach including electric and magnetic fields and how the known results for particles with quadratic dispersion can be translated into the specific linear dispersion of graphene. Then we discuss the currents in section III. From the linearization of the kinetic equation we get the response function for the coupled density and spin response with respect to an external electric field. In section V we discuss the intraband and interband conductivity in detail with various limiting ranges. There we generalize known results now including magnetic fields, magnetic domains and meanfields. The comparison of the longitudinal optical conductivity is presented and the Hall conductivity is discussed. Section VI contains the spin conductivity and shows a subtlety in using the infinite-mass limit in that contrary to the particle current the normal quasiparticle spin current does not vanish. Finally section VII explores the region where the effectively screened Coulomb repulsion between electrons is changing sign opening the possibility to form Cooper pairs. The summary concludes the paper.

II. KINETIC THEORY

We consider an effective Hamiltonian possessing a Pauli structure

$$\hat{H}_{\text{eff}} = H + \vec{\sigma} \cdot \vec{\Sigma} \quad (5)$$

with the Pauli matrices $\vec{\sigma}$ and the scalar Hamiltonian

$$H = \frac{p^2}{2m} + \Sigma_0(\vec{p}, \vec{r}, t) + e\Phi(\vec{r}, t) \quad (6)$$

consisting of a quadratic dispersion of particles and scalar meanfield selfenergy Σ_0 , the scalar e.m. potential Φ and the vector potential absorbed in the canonical momentum $\vec{p} = \vec{k} - e\vec{A}$. Any spin-orbit coupling \vec{b} and magnetic field \vec{B} can be written compactly as¹⁷

$$\vec{\Sigma} = \vec{\Sigma}^H(\vec{p}, \vec{r}, t) + \vec{b}(\vec{p}) + \mu_B \vec{B}. \quad (7)$$

For single-layer graphene we have $\vec{b} = v(p_x, p_y, 0)$ and the limit of $m \rightarrow \infty$. We will use this procedure to see how the results for spin-orbit coupled systems of^{17,42} translate into graphene. The (pseudo)spin-Hall effect in graphene itself is also investigated⁴³ reporting the anomalous Hall

effect in single-layer and bilayer graphene^{44,45} and which is treated like a spin-orbit coupled system⁴⁶ too.

The Wigner distribution function consists now of a scalar and a vector part

$$\hat{\rho}(\vec{p}, \vec{r}, t) = \langle \Psi^+ \Psi \rangle = f \hat{I} + \vec{\sigma} \cdot \vec{g} = \begin{pmatrix} f + g_z & g_x - i g_y \\ g_x + i g_y & f - g_z \end{pmatrix} \quad (8)$$

with (4) and the spinor creation operator $\Psi^+ = (\Psi_\uparrow^+, \Psi_\downarrow^+)$. The meanfield selfenergies read¹⁷

$$\begin{aligned} \Sigma_0(p, q, t) &= n(q, t) V_0(q) + \vec{s}(q, t) \cdot \vec{V}(q) \\ \vec{\Sigma}(p, q, t) &= \vec{s}(q, t) V_0(q) + n(q, t) \vec{V}(q) \end{aligned} \quad (9)$$

where \vec{V} describes the averaged magnetized domains or magnetic impurities (3).

The exact kinetic equations for this mean-field Hamiltonian consist of two coupled equations¹⁷

$$\begin{aligned} D_T f + \vec{A} \cdot \vec{g} &= 0 \\ D_T \vec{g} + \vec{A} \vec{f} &= 2(\vec{\Sigma} \times \vec{g}) \end{aligned} \quad (10)$$

where $D_T = (\partial_T + \vec{F} \partial_k + \vec{v} \partial_R)$ describes the drift and force of the scalar and vector part with the velocity

$$v = \frac{k}{m_e} + \partial_k \Sigma_0 \quad (11)$$

and the effective Lorentz force

$$\vec{F} = (e\vec{E} + e\vec{v} \times \vec{B} - \partial_R \Sigma_0). \quad (12)$$

The coupling between spinor parts is given by the vector drift

$$A_i = (\vec{\partial}_k \Sigma_i \vec{\partial}_R - \vec{\partial}_R \Sigma_i \vec{\partial}_k + e(\vec{\partial}_k \Sigma_i \times \vec{B}) \vec{\partial}_k). \quad (13)$$

Remember that we have subsumed in the vector selfenergy (7) the magnetic impurity meanfield, the spin-orbit coupling vector, and the Zeeman term.

The term (13) in the second parts on the left sides of (10) represents the coupling between the spin parts of the Wigner distribution. The vector part contains additionally the spin-rotation term on the right hand side. One has to consider additionally collision integrals. In the simplest way we will add a relaxation time with conserving Mermin's correction^{47,48}.

The stationary solution of (10) has the structure¹⁷

$$\hat{\rho}(\hat{\epsilon}) = \sum_{\pm} \hat{P}_{\pm} f_{\pm} = \frac{f_+ + f_-}{2} + \vec{\sigma} \cdot \vec{e} \frac{f_+ - f_-}{2} \equiv \rho + \vec{\sigma} \cdot \vec{\rho} \quad (14)$$

with $f_{\pm} = f_0(\epsilon_k(R) \pm |\vec{\Sigma}(k, R)|)$ and f_0 the Fermi-Dirac distribution. We obtain obviously a splitting of quasiparticle energies due to spin-orbit coupling

$$\epsilon_{\pm} = \frac{p^2}{2m} \pm |\vec{\Sigma}(k, R)| \rightarrow \pm v p \quad (15)$$

which takes the form of single-layer graphene for $m \rightarrow \infty$ and vanishing magnetic field $\vec{\Sigma} = \vec{b} = v\vec{p}$. This supports the idea to represent the single-layer graphene simply by the limit of infinite mass as illustrated in figure 1 and used in¹⁶.

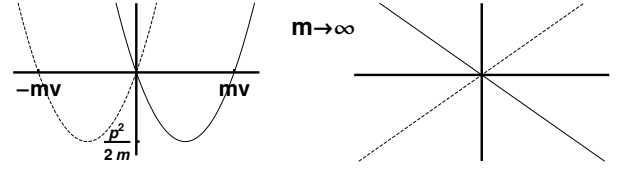


FIG. 1. Realization of linear Dirac dispersion of graphene by the infinite-mass limit of spin-orbit coupled system with quadratic dispersion.

III. CURRENTS

Due to the spin-orbit coupling (7) the current possesses a normal and anomaly part. Using $[\vec{b}(\vec{p}), \vec{x}] = -i\hbar \partial_{\vec{p}} \vec{b}(\vec{p})$ from elementary quantum mechanics we have

$$\hat{v}_j = \frac{i}{\hbar} [\hat{H}, \hat{x}_j] = \partial_{p_j} \epsilon + \partial_{p_j} \vec{b} \cdot \vec{\sigma} \quad (16)$$

if the single particle Hamiltonian is given by the quasiparticle energy $\epsilon(p)$. Together with the Wigner function (8) one has

$$\hat{\rho} \hat{v}_j = f \partial_{p_j} \epsilon + \vec{g} \cdot \partial_{p_j} \vec{b} + \vec{\sigma} \cdot (\partial_{p_j} \epsilon \vec{g} + f \partial_{p_j} \vec{b} + i \partial_{p_j} \vec{b} \times \vec{g}) \quad (17)$$

and the particle and spin current densities read

$$\begin{aligned} \hat{J}_j &= \sum_p [\hat{\rho}, v_j]_+ \\ &= 2 \sum_p \left[f \partial_{p_j} \epsilon + \vec{g} \cdot \partial_{p_j} \vec{b} + \vec{\sigma} \cdot (\partial_{p_j} \epsilon \vec{g} + f \partial_{p_j} \vec{b}) \right] \\ &= J_j + \vec{\sigma} \cdot \vec{S}_j. \end{aligned} \quad (18)$$

The scalar part describes the particle current $\vec{J} = \vec{J}^n + \vec{J}^a$ consisting of a normal and anomaly current and the vector part describes the spin current S_{ij} not to be confused with the polarization \vec{s} .

In the limit of infinite mass, $\epsilon_p \rightarrow 0$ and therefore $\partial_{p_j} \epsilon \rightarrow 0$ we obtain that graphene can only possess an anomalous particle current since the normal one would be of Drude type vanishing for $m \rightarrow \infty$. The normal spin current, however, possesses a finite $m \rightarrow \infty$ limit which is unexpected. This we will treat in section VI.

Lets first consider the particle current. In¹⁷ the linearized solution of (10) has been derived which reads in the long-wavelength limit $[E \partial_p = \vec{E} \cdot \vec{\partial}_p]$

$$\begin{aligned} \delta \vec{g}(\omega, p) &= \frac{i\omega}{4|\Sigma|^2 - \omega^2} e E \partial_p \vec{g} \\ &\quad - 2 \frac{1}{4|\Sigma|^2 - \omega^2} \vec{\Sigma} \times e E \partial_p \vec{g} \\ &\quad - 4i \frac{1}{\omega(4|\Sigma|^2 - \omega^2)} \vec{\Sigma} (\vec{\Sigma} \cdot e E \partial_p \vec{g}). \end{aligned} \quad (19)$$

From the three terms in (19) we get the symmetric and

asymmetric conductivity¹⁷. One has according to (18)

$$\delta j_\alpha = \sum_p \partial_{p_\alpha} \vec{\Sigma} \cdot \delta \vec{g} = \sum_p \Sigma \partial_{p_\alpha} \vec{e} \delta \vec{g} + \sum_p \vec{e} (\vec{e} \partial_{p_\alpha} \vec{\Sigma}). \quad (20)$$

Writing $j_\alpha = \sigma_{\alpha\beta} E_\beta$ we obtain from the first part of (20) using (19) the interband and the anomalous Hall conductivity

$$\begin{aligned} \sigma_{\alpha\beta}^{\text{inter}} &= 2e^2 \sum_p \frac{g}{1 - \frac{\omega^2}{4|\Sigma|^2}} \frac{i\omega}{2|\Sigma|} \partial_\alpha \vec{e} \cdot \partial_\beta \vec{e} \\ \sigma_{\alpha\beta}^{\text{Hall}} &= 2e^2 \sum_p \frac{g}{1 - \frac{\omega^2}{4|\Sigma|^2}} \vec{e} \cdot (\partial_\alpha \vec{e} \times \partial_\beta \vec{e}) \end{aligned} \quad (21)$$

where the first part of (19) leads to the interband and the second part of (19) to the Hall conductivity.

The second part of (20) with (19) leads to the intraband conductivity

$$\sigma_{\alpha\beta}^{\text{intra}} = i2e^2 \sum_p \partial_\alpha \partial_\beta \Sigma \frac{g}{\omega} \quad (22)$$

where the first and the third part of (19) contributes. This intraband contribution had been neglected in¹⁷.

The anomalous charge current reads

$$\begin{aligned} \delta \vec{j}(t) &= 2ev \sum_p \delta \vec{g} = -2ev \sum_p \int_0^t d\bar{t} e^{-\frac{t-\bar{t}}{\tau}} \left\{ \cos(2vp\bar{t}) E_{t-\bar{t}} \partial_p \vec{g} \right. \\ &\quad \left. + \sin(2vp\bar{t}) \vec{p}_0 \times E_{t-\bar{t}} \partial_p \vec{g} + [1 - \cos(2vp\bar{t})] [\vec{p}_0 \cdot E_{t-\bar{t}} \partial_p \vec{g}] \vec{p}_0 \right\}. \end{aligned} \quad (23)$$

Each term from (19) corresponds to a specific precession motion analogously to the one seen in the conductivity of a charge in crossed electric and magnetic fields if we replace $\omega_c = eB/m \leftrightarrow 2|\Sigma| = 2vp$

$$\begin{aligned} \delta \vec{j}(t) &= \sigma_0 \int_0^t \frac{d\bar{t}}{\tau} e^{-\frac{t-\bar{t}}{\tau}} \left\{ \cos(\omega_c \bar{t}) \vec{E}(t-\bar{t}) \right. \\ &\quad \left. + \sin(\omega_c \bar{t}) \vec{E}(t-\bar{t}) \times \vec{B}_0 + [1 - \cos(\omega_c \bar{t})] [\vec{E}(t-\bar{t}) \cdot \vec{B}_0] \vec{B}_0 \right\} \end{aligned} \quad (24)$$

as the solution of the Newton equation of motion

$$m_e \dot{\vec{v}} = e(\vec{v} \times \vec{B}) + e\vec{E} - m_e \frac{\vec{v}}{\tau}. \quad (25)$$

This illustrates the threefold orbiting of the electrons with cyclotron frequency: (i) in the direction of the electric and (ii) magnetic field, and (iii) in the direction perpendicular to the magnetic and electric field.

One can find these 3 terms also directly solving the Heisenberg equation for the spinor creation operators from the free graphene Hamiltonian

$$v \sum_p \Psi_p^\dagger \vec{\sigma} \cdot \vec{p} \Psi_p \quad (26)$$

which reads¹⁹

$$\Psi_t = \left[\cos(vpt) - i \frac{\vec{\Sigma} \cdot \vec{p}}{p} \sin(vpt) \right] \Psi_p. \quad (27)$$

The charge current operator (16) is calculated directly¹⁹ with (27)

$$\begin{aligned} \hat{j} &= ev \sum_p \Psi_t^\dagger \vec{\sigma} \Psi_t \\ &= ev \sum_p \Psi_p^\dagger [\cos(2vpt) \vec{\sigma} + (1 - \cos(2vpt)) (\vec{\sigma} \cdot \vec{p}) \vec{p} \\ &\quad + \sin(2vpt) (\vec{p} \times \vec{\sigma})] \Psi_p. \end{aligned} \quad (28)$$

We use now the ensemble average

$$\langle \Psi_\alpha^\dagger \vec{\sigma}_{\alpha\beta} \Psi_\beta \rangle = \vec{\sigma}_{\alpha\beta} (f_0 \delta_{\alpha\beta} + \vec{\sigma}_{\beta\alpha} \times \vec{g}_0) = 2\vec{g}_0 \quad (29)$$

with the Wigner function (8) we obtain exactly (23) with $\vec{g}_0 = eE \partial_p \vec{g}$. There is no reason to call the last term in (28) an expression of Zitterbewegung as claimed in¹⁹.

IV. RESPONSE FUNCTIONS

If one linearizes the kinetic equation (10) with respect to an external electric potential Φ one obtains the equation system for density and spin responses⁴²

$$\begin{aligned} \left(1 - \frac{i}{\bar{\omega}\tau}\right) \delta n &= \Pi_0 (\delta \Sigma + \Phi) + \vec{\Pi} \cdot \delta \vec{\Sigma} + \sum_p \frac{q \partial_p \vec{\Sigma} \cdot \delta \vec{g}}{\bar{\omega}} \\ \delta \vec{s} &= \vec{\Pi}_3 (\delta \Sigma + \Phi) + \vec{\Pi}_2 \times \delta \vec{\Sigma} + \Pi_0 \delta \vec{\Sigma} + \overleftrightarrow{\vec{\Pi}} \cdot \delta \vec{\Sigma} \end{aligned} \quad (30)$$

for any spin-orbit coupling where the different polarization functions are given in⁴², $\bar{\omega} = \omega - \vec{p} \cdot \vec{q}/m + i/\tau$, $\bar{\omega} = \omega + i/\tau$, and the intrinsic mean field variations read

$$\begin{aligned} \delta \vec{\Sigma} &= \vec{V} \delta n + V_0 \delta \vec{s} \\ \delta \Sigma &= \vec{V} \cdot \delta \vec{s} + V_0 \delta n. \end{aligned} \quad (31)$$

Here we represent any interaction of electrons with scalar impurities or among themselves by the potential V_0 and with magnetic impurities by the potential \vec{V} . The latter allows to include averaged magnetization domains. The term on the left hand side of (30) in front of the density variation is a result of Mermin's correction^{47,48} and crucial for conserving relaxation time approximation.

For graphene in the infinite-mass limit the response functions take the form $\Pi_0 = \vec{\Pi} = 0$ and

$$\begin{aligned} \vec{\Pi}_3 &= \frac{2i\Sigma_n \lambda}{v\bar{\omega}} \mathcal{E} \vec{e}_z \times \vec{q} - \frac{4\lambda^2}{\bar{\omega}} \mathcal{C} \vec{q} \\ \vec{\Pi}_2 &= -\frac{2i\Sigma_n}{v\bar{\omega}} \mathcal{E} \vec{e}_z - \frac{i\lambda}{\bar{\omega}} \mathcal{F} \vec{q} \\ \overleftrightarrow{\vec{\Pi}} \cdot \delta \vec{\Sigma} &= -\frac{4\lambda}{\bar{\omega}} \left(\mathcal{C} \delta \vec{\Sigma}_\perp + \tilde{\mathcal{C}} \delta \Sigma_z \vec{e}_z \right) \\ &\quad + \frac{2\lambda^2 \Sigma_n}{v\bar{\omega}} \mathcal{F} \left(\delta \Sigma_z \vec{q} + (\vec{q} \cdot \delta \vec{\Sigma}) \vec{e}_z \right). \end{aligned} \quad (32)$$

We used $\lambda = v/\bar{\omega}\hbar$, $|\vec{\Sigma}| = v\Gamma$ with $\Gamma^2 = p^2 + (\Sigma_n/v)^2$, and the effective Zeeman field in z -direction

$$\Sigma_n = |n\vec{V} + \vec{s}\vec{V}_0 + \mu_B\vec{B}|. \quad (33)$$

The direction of spin is $\vec{e} = (p_x, p_y, \frac{\Sigma_n}{v})/\Gamma$, and the used integrals read performing angular integrations

$$\begin{aligned} \mathcal{A} &= \sum_p \frac{g}{\Gamma} \left(1 - \frac{p^2}{2\Gamma^2}\right) = -\sum_p \frac{p^2}{2\Gamma^2} f' = -\mathcal{D}, \\ \mathcal{B} &= \sum_p \frac{g}{\Gamma} \frac{1 - \frac{p^2}{2\Gamma^2}}{1 - 4\lambda^2\Gamma^2} = \mathcal{A} + 4\lambda^2\mathcal{C}, \\ \mathcal{C} &= \sum_p \frac{g\Gamma \left(1 - \frac{p^2}{2\Gamma^2}\right)}{1 - 4\lambda^2\Gamma^2}, \quad \tilde{\mathcal{C}} = \sum_p \frac{g\Gamma \left(1 - \frac{B^2}{\Gamma^2}\right)}{1 - 4\lambda^2\Gamma^2}, \\ \mathcal{E} &= \sum_p \frac{g}{\Gamma(1 - 4\lambda^2\Gamma^2)}, \quad \mathcal{F} = \sum_p \frac{p^2 g'}{\Gamma(1 - 4\lambda^2\Gamma^2)} \end{aligned} \quad (34)$$

with $f' = v\partial_\epsilon f$. The nontrivial identity in the first line can be shown from $\sum_p (\vec{q} \cdot \vec{\partial}_p) \vec{g} = 0$. The forms (34) are convenient objects for numerical evaluation at finite temperatures. Please note that these forms are much more rich than the pure mean-field free polarizations found in⁴⁹.

While \mathcal{A} and \mathcal{C} seem to be divergent needing a cut-off due to unbounded hole states, \mathcal{B} is convergent. However, \mathcal{D} is convergent as seen below which illustrates the delicate compensation of divergences in \mathcal{A} and \mathcal{C} due to the angular integration. Actually, inspecting (34) it seems that due to f_- the \mathcal{A} term is divergent for large momenta. Usually this has been regularized by an upper momentum cut-off representing the band width. Lets inspect how this procedure appears in the density n and polarization s

$$n/s = \frac{1}{2} \sum_p (f_+ \pm f_-) \quad (35)$$

with $f_\pm = (1 + e^{\frac{\pm v p - \mu}{T}})^{-1}$. The upper integration limit of f_- diverges. One interprets $1 - f_- = (1 + e^{\frac{vp + \mu}{T}} + 1)^{-1} = f_h$ as the distribution of holes^{50,51} which splits the density into the baryon density $n_p - n_h$

$$n/s = n_p \mp n_h \pm \frac{\lambda^2}{8\pi\hbar^2} \quad (36)$$

and a part given by the whole momentum sum with the upper momentum cut-off λ . At zero temperatures we have in two dimensions

$$n(T=0) = n_p = s = \frac{\mu^2}{8\pi\hbar^2 v^2} \quad (37)$$

with the chemical potential (Fermi energy) μ .

This regularization seems to be applicable to the expression \mathcal{A} as done in the literature. However, there is a delicate balance rendering this integral finite without regularization due to the identity expressing \mathcal{A} by the obviously converging expression \mathcal{D} . Lets inspect the structure

of this term by splitting off a convergent magnetic-field-dependent part

$$\begin{aligned} \mathcal{D} &= \frac{v}{2} \sum_p \frac{p^2}{\Gamma^2} \partial_\epsilon f \\ &= \frac{v}{2} \sum_p \partial_\epsilon f - \frac{\Sigma_n^2}{2v} \sum_p \frac{\partial_\epsilon f}{\Gamma^2} \\ &= -\frac{v}{2} \partial_\mu n - \frac{\Sigma_n^2}{2v} \sum_p \frac{\partial_\epsilon f}{\Gamma^2}. \end{aligned} \quad (38)$$

This shows that the divergent part is represented by the compressibility. Assuming that this momentum cut-off is solely given by the band width and not dependent on the density, i.e. chemical potential, we get the first part of (38) analytically

$$\begin{aligned} -\frac{v}{2} \partial_\mu n &= \frac{1}{4\pi\hbar^2} \left\{ -\Sigma_n \frac{\sinh \frac{\Sigma_n}{T}}{\cosh \frac{\mu}{T} + \cosh \frac{\Sigma_n}{T}} \right. \\ &\quad \left. + T \ln \left[2(\cosh \frac{\mu}{T} + \cosh \frac{\Sigma_n}{T}) \right] \right\}. \end{aligned} \quad (39)$$

The cancellation of the divergence comes here due to the angular integration.

V. CONDUCTIVITY

A. Longitudinal conductivity

The interband and intraband (21) conductivities provide both parts of the longitudinal conductivity

$$\sigma_{xx} = -ie^2 2\lambda(\mathcal{B} + \mathcal{D}) \quad (40)$$

where the first part is the interband and the second part the intraband contribution. We will discuss both parts separately.

First we prove the internal consistency of the theory by deriving the conductivity from the response function. The conductivity is defined as the response with respect to the internal field which means we have to consider the response without meanfields, i.e. the polarization function $\Pi = \delta n(\Sigma = 0)/\Phi$. Then (30) reduces to

$$\begin{aligned} \left(1 - \frac{i}{\bar{\omega}\tau}\right) \delta n &= \lambda \vec{q} \cdot \vec{\delta s} \\ \delta \vec{s} &= \vec{\Pi}_3 \Phi \end{aligned} \quad (41)$$

which yields with (32) exactly the current (23). As a cross check we use for V_0 the Coulomb potential. From the Maxwell equation the longitudinal conductivity is expressed as

$$\sigma_{xx} = -\epsilon_0 \omega V_0 \text{Im} \Pi \quad (42)$$

and from (41)

$$\sigma_{xx} = -\epsilon_0 \omega V_0 \text{Im} \left(-\frac{4\lambda^3 \mathcal{C} q^2}{\bar{\omega} - \frac{i}{\tau}} \right) = 4e^2 l_D \mathcal{C} v^3 \text{Im}(i\tau\omega^3) \quad (43)$$

| order of limits | | | | | $\sigma_{xx}^B = \zeta \frac{e^2}{16\hbar}$ |
|-----------------|----------|----------|----------|----------|---|
| μ | ω | Σ | m | τ | -1 |
| μ | τ | Σ | m | ω | 0 |
| τ | μ | Σ | m | ω | 1 |
| μ | Σ | τ | m | ω | 1 |
| μ | τ | m | Σ | ω | 1 |
| μ | Σ | m | τ | ω | 0 |
| μ | m | τ | Σ | ω | 0 |
| μ | m | Σ | ω | τ | 0 |
| μ | Σ | ω | m | τ | 0 |

TABLE I. results for different orders of limits.

with

$$\tau_\omega = \frac{\tau}{(1 - i\omega\tau)} \quad (44)$$

and $l_D = 1$ for three dimensions and $l_D = q/2\hbar$ for quasi-two dimensions⁵². For the static limit one gets exactly the result from current formula (40) since $\mathcal{B} + \mathcal{D} = \mathcal{B} - \mathcal{A} = 4\lambda^2\mathcal{C}$. This illustrates ones more the necessity to include Mermin's corrections^{47,48} represented by the left side subtraction in (30) or (41).

1. Interband conductivity

The zero-temperature limit of the interband part considered in¹⁷ reads for particles with quadratic dispersion

$$\sigma_{xx}^B = -ie2\lambda\mathcal{B} = \frac{e^2}{8\pi\hbar} \left\{ \frac{4\epsilon_v\Sigma_n^2\tau_\omega/\hbar}{2\epsilon_v\mu + \Sigma_n^2} + \left(1 - \frac{4\Sigma_n^2\tau_\omega^2}{\hbar^2}\right) \arctan \left[\frac{4\epsilon_v\tau_\omega\hbar}{\hbar^2 + 4(2\epsilon_v\mu + \Sigma_n^2)\tau_\omega^2} \right] \right\} \quad (45)$$

with $\epsilon_v = mv^2/\hbar$. This conductivity represents a contribution in the direction of the applied electric field and is caused by collisional correlations. This dynamical result is different from the spin accumulation found in⁵³ basically by the \arctan term and therefore no sharp resonance feature. Expanding, however, in small spin-orbit coupling

$$\sigma_{xx}^B = \frac{e^2}{\pi\hbar} \frac{\epsilon_v\tau_\omega}{1 + 4\Sigma_n^2\tau_\omega^2} + o(\epsilon_v^2) \quad (46)$$

shows that the static limit agrees with^{53,54}. Please note that if one sets $\Sigma_n \rightarrow 0$ before expanding a factor $1/2$ appears which illustrates the symmetry breaking by the effective Zeeman term.

To translate (45) into the formula for graphene we perform the limit of infinite mass or $\epsilon_v \rightarrow \infty$. The order of limits becomes now essential as illustrated in table I: the vanishing Zeemann field $\Sigma_n \rightarrow 0$ denoted by Σ , the static

limit denoted by ω , the infinite-mass limit denoted by m , and the zero-density limit denoted by μ . If we apply the limit of vanishing friction $\tau^{-1} \rightarrow 0$ before the infinite-mass limit we obtain $\sigma_{xx}^B = 0$ and if we perform the static limit even afterward we obtain the negative result of the expected one (2). Performing correctly first the infinite-mass limit we get for zero temperature

$$\sigma_{xx}^B = \frac{e^2}{8\pi\hbar} \begin{cases} \frac{2\Sigma_n^2\tau_\omega}{\hbar\mu} + \left(1 - \frac{4\Sigma_n^2\tau_\omega^2}{\hbar^2}\right) \operatorname{arccot} \frac{2\mu\tau_\omega}{\hbar}, & \mu > \Sigma \\ \frac{2\Sigma_n\tau_\omega}{\hbar} + \left(1 - \frac{4\Sigma_n^2\tau_\omega^2}{\hbar^2}\right) \operatorname{arccot} \frac{2\Sigma_n\tau_\omega}{\hbar}, & \mu < \Sigma \end{cases} \quad (47)$$

Since (44) the limits of infinite frequency $\omega \rightarrow \infty$, vanishing scattering $\tau \rightarrow \infty$, and vanishing density are not interchangeable as well. In fact, if we neglect the Zeeman field, $\Sigma_n = 0$, in (47) we get

$$\sigma_{xx}^B = \frac{e^2}{16\hbar} \begin{cases} -1 - i\frac{4\mu}{\pi\hbar\omega} + o\left(\frac{1}{\omega^2}\right) \\ 1 - \frac{4}{\pi\hbar} \frac{\mu\tau}{\omega\tau+i} + o(\mu^2) \\ -1 - i\frac{4\mu}{\pi\hbar\omega} + o(\mu^2) + o\left(\frac{1}{\tau}\right) \\ 0 + o(\omega) + o\left(\frac{1}{\tau}\right) \\ 1 + o\left(\frac{1}{\tau}\right) + o(\omega) \end{cases} \quad (48)$$

Only the second limiting procedure leads to the right result. One obtains even zero value if the static limit is used after vanishing scattering which is different from interchanging both limits. This illustrates the care one has to take when integrating zero-temperature values.

The finite-temperature interband conductivity can be written with \mathcal{B} from (34) as

$$\sigma_{xx}^B = \frac{e^2 T \tau_\omega}{4\pi\hbar^2} \int_{\Sigma/T}^{\infty} dx \frac{1 + \left(\frac{\Sigma_n}{T}\right)^2}{1 + \frac{4x^2 T^2 \tau_\omega^2}{\hbar^2}} \left(\frac{1}{e^{\frac{-x-\mu}{T}} + 1} - \frac{1}{e^{\frac{x-\mu}{T}} + 1} \right) \quad (49)$$

which is plotted in figure 2.

Please note that the frequency dependence is solely due to (44). We see that the interband conductivity approaches the universal value σ_2 of (2) in the case of no Zeeman field and $T = 0$ as can be seen in (48). For finite Zeeman fields even at zero temperature this universal value is different which rises doubts to call it universal value. As seen in figure 2 from (47) the finite Zeeman field introduces a density threshold below which the interband conductivity is nearly constant.

The real part of interband conductivity can be given analytically for small scattering $\tau^{-1} \rightarrow 0$ where one uses $1/(\omega + i\epsilon) = P/\omega - i\pi\delta(\omega)$. One obtains a nonzero result only for $\hbar\omega > 2\Sigma_n$ which reads

$$\begin{aligned} \operatorname{Re}\sigma_{xx}^B &= -\frac{e^2}{16\hbar} \left(1 + \frac{4\Sigma_n^2}{\hbar^2\omega^2}\right) \left(\frac{1}{e^{\frac{\hbar\omega-\mu}{2T}} + 1} - \frac{1}{e^{\frac{-\hbar\omega-\mu}{2T}} + 1} \right) \\ &= \frac{e^2}{16\hbar} \left(1 + \frac{4\Sigma_n^2}{\hbar^2\omega^2}\right) \frac{\sinh \frac{\hbar\omega}{2T}}{\cosh \frac{\mu}{T} + \cosh \frac{\hbar\omega}{2T}} \\ &\approx \frac{e^2}{16\hbar} \left(1 + \frac{4\Sigma_n^2}{\hbar^2\omega^2}\right) \tanh \frac{\hbar\omega}{2T}, \quad \omega > 2\mu \gg T. \end{aligned} \quad (50)$$

The last expression without Zeeman field Σ_n has been given by⁵⁵ with a misprint of 1/4 in the argument. The second line was found in⁵⁶ within a Kubo formalism also without Σ_n . An extension of this result towards trigonal-warping corrections and bilayer graphene can be found in⁵⁷.

Due to the abbreviated dynamical relaxation time (44) we can now discuss the frequency dependence. For zero temperature we use from (47) the case of $\mu > \Sigma_n$ since in the opposite limit one simply replaces $\mu \rightarrow \Sigma_n$ in the expression and obtains

$$\sigma_{xx}^B = \frac{e^2}{8\pi\hbar} \left[\frac{2\Sigma_n^2 i}{\mu\hbar(\omega + \frac{i}{\tau})} + \frac{i}{2} \left(1 + \frac{4\Sigma_n^2}{\hbar^2(\omega + \frac{i}{\tau})^2} \right) \ln \frac{2\mu - \hbar(\omega + \frac{i}{\tau})}{2\mu + \hbar(\omega + \frac{i}{\tau})} \right]. \quad (51)$$

If we neglect the Zeeman field $\Sigma_n \rightarrow 0$ and consider the limit of vanishing collisions $\tau \rightarrow \infty$ we obtain the result

$$\sigma_{xx}^B = \frac{e^2}{16\hbar} \left[\Theta(\hbar\omega - 2\mu) + \frac{i}{\pi} \ln \left| \frac{\hbar\omega - 2\mu}{\hbar\omega + 2\mu} \right| \right] \quad (52)$$

which is exactly the result reviewed in⁵⁸ with a misprint of missing i and which has been first derived by⁵⁹ and within RPA in⁶⁰. It was extended by selfconsistent Born approximation in⁶¹ and including circularly polarized light⁶². The Kubo formalism leads to the same expression⁶³. The interband conductivity (52) shows a singularity at the interband transition energy $\hbar\omega = 2\mu$ which is damped by collisions and finite temperatures.

Here we have extended the known expressions by the effective Zeeman field including the magnetic field, magnetized domains, and meanfields.

2. Intraband contribution

We have seen that the interband contribution leads to the universal low-density conductivity at zero temperature and decreases with higher densities. Now we will discuss the intraband contribution which vanishes for zero temperature and low densities. In¹⁷ we have neglected this term (22) corresponding to the \mathcal{D} intraband conductivity in (40). This is not justified for graphene since this term is just the intraband scattering and will lead to the linear density dependence.

The finite-temperature expression of the part (40) of conductivity reads explicitly

$$\begin{aligned} \sigma_{xx}^D &= -ie^2 2\lambda D \\ &= \frac{e^2 T \tau_\omega}{4\pi\hbar^2} \int_{\frac{\Sigma_n}{T}}^{\infty} dx \left(\frac{\Sigma_n^2}{T^2} - x^2 \right) \left[\frac{1}{\left(e^{\frac{x-\mu}{T}} + 1 \right) \left(e^{\frac{-x+\mu}{T}} + 1 \right)} + (\mu \leftrightarrow -\mu) \right] \\ &= \frac{i\epsilon_0 \omega_p^2}{\omega + \frac{i}{\tau}}. \end{aligned} \quad (53)$$

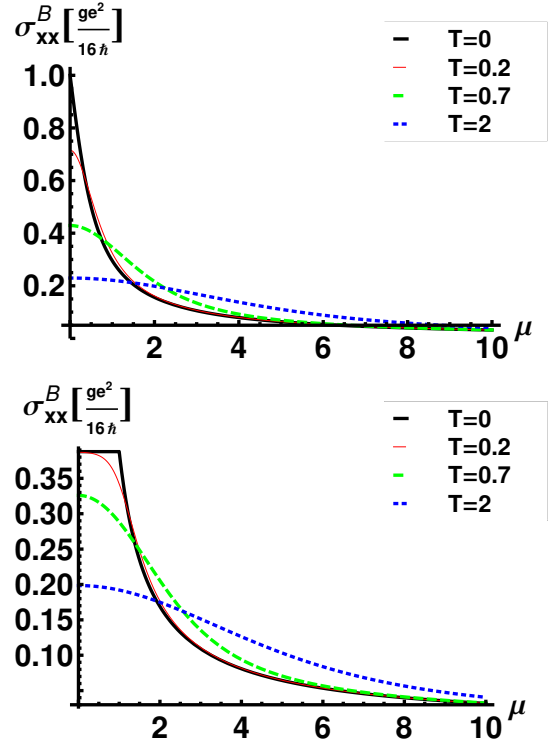


FIG. 2. Temperature dependence (in arbitrary energy units EU) of static interband (49) conductivity with $\Sigma_n = 0$ (above) and $\Sigma_n = 1EU$ (below) with $\tau = \hbar/EU$ versus the chemical potential in units EU.

Consequently, this intraband contribution can be written in the form of the frequency-dependent Drude conductivity with a collective frequency $\omega_p[\mu, T, \Sigma_n]$ dependent on the chemical potential, temperature and effective Zeeman field. It is illustrated in figures 3 for different temperatures versus chemical potential. Except the factor $\tau_\omega \epsilon_0$ the figures 3 give therefore also the collective mode squared. One sees that the mode is excited for zero temperature only for $\mu > \Sigma_n$ which provides a threshold for densities by the effective Zeeman field. In fact, we have for zero-temperature

$$\sigma_{xx}^D = \frac{e^2 \tau_\omega}{4\pi\hbar^2} \frac{\mu^2 - \Sigma_n^2}{\mu} \Theta(\mu - \Sigma_n) \quad (54)$$

starting at chemical potentials (Fermi energies) larger than the effective Zeeman field Σ_n seen in figures 3.

If we neglect the effective Zeeman field $\Sigma_n \rightarrow 0$, the expression (53) takes exactly the form of intraband contribution discussed in⁵⁵. Therefore we can consider the expression (53) as generalization of the known result including now the magnetic field and the meanfields.

One sees that for finite temperatures the intraband conductivity is approaching a finite value for low densities. However for zero temperature this limit vanishes. Therefore the "universal" limit discussed in the literature concerns solely the intraband contribution. We can state that any finite temperature will blur this univer-

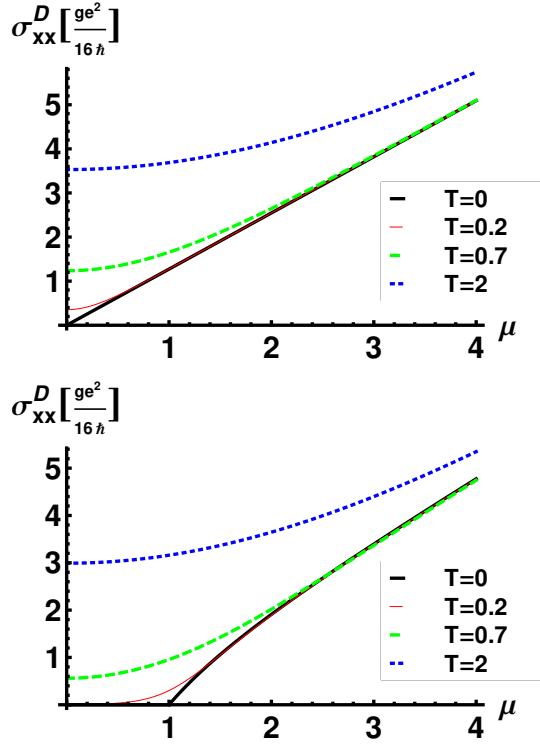


FIG. 3. Temperature dependence (in arbitrary energy units EU) of the static intraband (53) conductivity with $\Sigma_n = 0$ (above) and $\Sigma_n = 1EU$ (below) and $\tau = \hbar/EU$ versus the chemical potential in units EU.

sal result since contributions start to contribute from the interband scattering.

The limit of vanishing effective Zeeman field can be given analytically as well and reads

$$\begin{aligned}\sigma_{xx}^D(\Sigma_n = 0) &= \frac{e^2\tau\omega}{4\pi\hbar^2} \left[2T \ln \left(1 + e^{\frac{\mu}{T}} \right) - \mu \right] \\ &= \frac{e^2\tau\omega T}{16\pi\hbar^2} \left(8 \ln 2 + \frac{\mu^2}{T^2} \right) + o\left(\frac{\mu}{T}\right)^4 \\ &= \frac{e^2\tau\omega\mu}{4\pi\hbar^2} + o\left(Te^{-\frac{\mu}{T}}\right)\end{aligned}\quad (55)$$

plotted in figure 3 as well.

The limit of high frequencies

$$\tau\omega = \frac{\tau}{1 - i\omega\tau} \approx \frac{i}{\omega} \quad (56)$$

and small densities $\mu \ll T$ has been first given in the framework of 3D graphite by⁶⁴ with a corresponding additional factor $2/d$ of inverse distance between the graphite layers. As special case of (55) without effective Zeeman fields, the high-frequency limit coincides with the result of⁵⁵.

In figure 4 finally we plot the complete static conductivity as a sum of (49) and (53). For zero temperature the universal finite value at low densities comes exclusively from the interband conductivity as discussed above. The

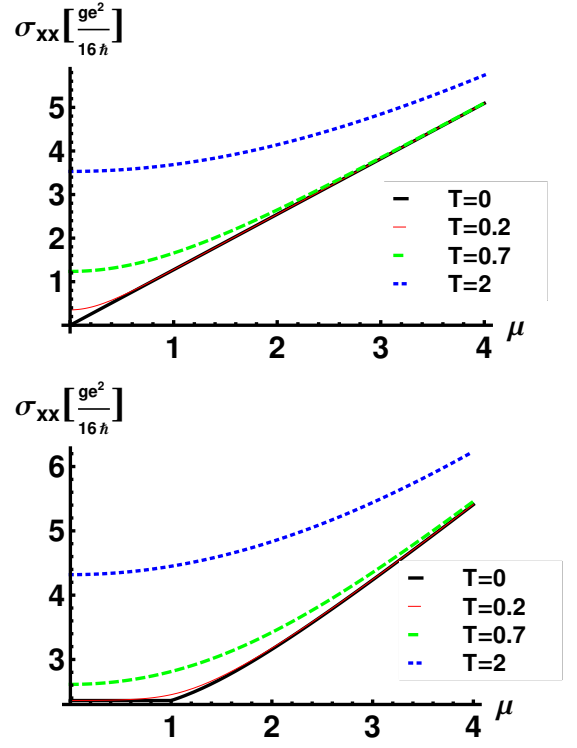


FIG. 4. Temperature dependence (in arbitrary energy units EU) of the total (40) static graphene conductivity with $\Sigma_n = 0$ (above) and $\Sigma_n = 1EU$ (below) and $\tau = \hbar/EU$ versus the chemical potential in units EU.

intraband conductivity has a threshold at the effective Zeeman field. Higher temperatures mixes both components and waves the threshold of intraband conductivity.

3. Optical conductivity: comparison with experiment

The optical conductivity $\sigma(\omega)$ is important to know if one wants to calculate the optical transparency⁶⁵

$$t(\omega) = \left[1 + \frac{\sigma(\omega)}{2\epsilon_0 c} \right]^{-2}. \quad (57)$$

We plot the optical conductivity at zero temperature as the sum of the interband (51) and intraband (54) conductivity and remember that the frequency dependence is given by (44). In figure 5 we see that the imaginary part of the optical conductivity possesses a minimum at the interband threshold corresponding to a step-like behavior of the real part of the conductivity. This feature is smeared out by scattering represented by a finite relaxation time. At high frequencies the optical conductivity approaches the universal value due to interband transitions (51).

If the effective Zeeman field becomes larger than the chemical potential (Fermi energy) than the conductivity is exclusively due to intraband transitions and indepen-

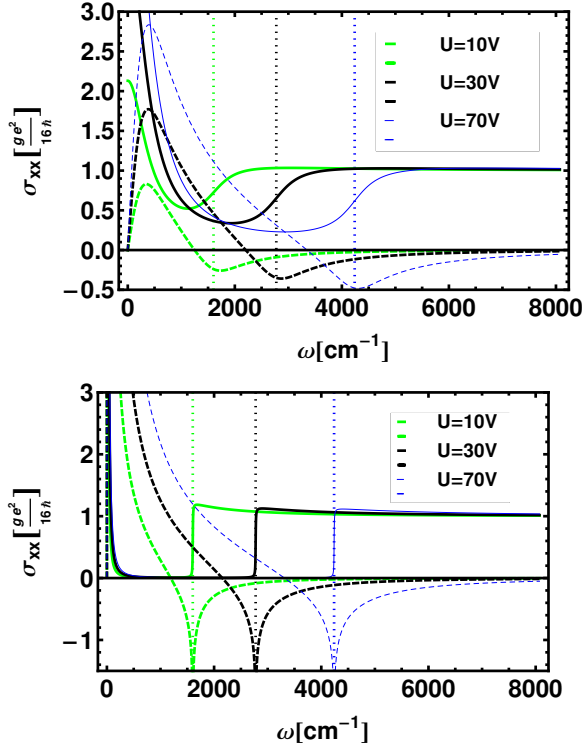


FIG. 5. Real (solid) and imaginary (dashed) optical conductivity versus frequency for $\tau = 20\hbar/eV$ (above) and $\tau = 2000\hbar/eV$ (below). The vertical dotted lines indicate the interband threshold $\hbar\omega = 2\mu$. The applied voltage induces a density $n = \frac{\epsilon\epsilon_0}{ed}U = 7.3 \times 10^{10} \text{cm}^{-2} \text{V}^{-1}U$ for graphene on typical SiO_2 substrates^{66,67}. The density is linked to the chemical potential $n = \frac{g\mu^2}{4\pi\hbar^2 v^2} = 1010 \text{cm}^{-2} (\mu/\text{eV})^2$.

dent of density according to (51)

$$\sigma_{xx}^B(\Sigma_n > \mu) = \frac{e^2}{8\pi\hbar} \left[\frac{4\Sigma_n i}{\hbar(\omega + \frac{i}{\tau})} + \frac{i}{\pi} \left(1 + \frac{4\Sigma_n^2}{\hbar^2(\omega + \frac{i}{\tau})^2} \right) \ln \frac{2\Sigma_n - (\omega + \frac{i}{\tau})}{2\Sigma_n + (\omega + \frac{i}{\tau})} \right] \quad (58)$$

seen in figure 6. The real part of the conductivity starts at the threshold $\hbar\omega = 2\Sigma_n$ accompanied by a minimum in the imaginary part. The finite scattering smears this step-like behavior and leads in the strong scattering limit to a constant real conductivity of universal value. The astonishing fact is that not only an universal value appears for small densities due to the chiral nature of particles but that a whole universal optical conductivity appears independent of density and solely determined by strong effective Zeeman fields.

In figure 7 we compare with the experimental data of⁶⁷. We find the best fit with the help of fitting the relaxation time and the effective Zeeman field presented in the next figure 8. One sees that the relaxation time decreases with increasing density and the effective Zeeman field

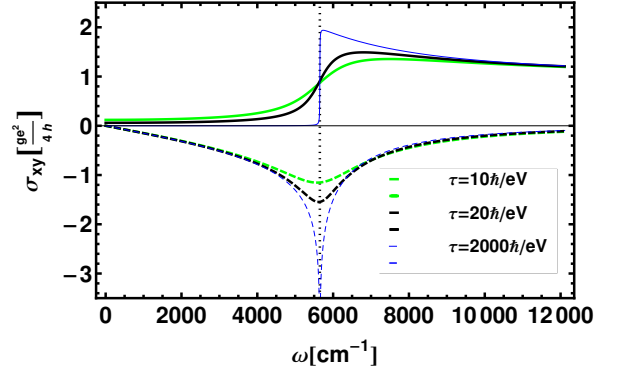


FIG. 6. Real (solid) and imaginary (dashed) optical conductivity versus frequency for different relaxation times which is independent of density (universal) for $\Sigma_n = 0.35 \text{eV} > \mu = 0.1 \text{eV}$. The vertical dotted lines indicate the interband threshold $\hbar\omega = 2\Sigma_n$.

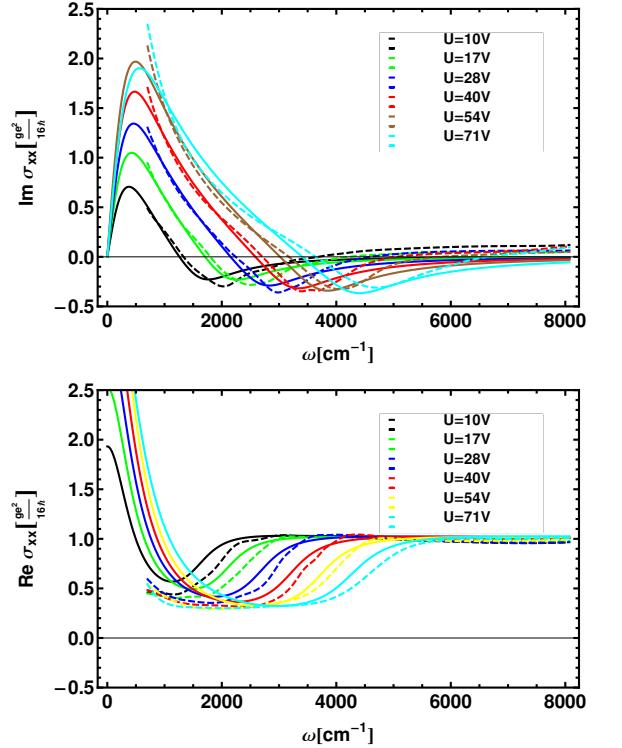


FIG. 7. (Color online) Real (above) and imaginary (below) optical conductivity versus frequency for different applied voltages compared with the experimental data (dashed) of⁶⁷. The parameters are given in figure 5.

increases. The found relaxation time is in agreement with the theoretical value of screened charged impurities of density n_s . The relaxation time reads⁶⁸

$$\frac{\hbar}{\tau} = \frac{n_s k_f}{2\pi\hbar^2 v} \int_0^{2\pi} d\theta V^2(q)(1 - \cos\theta) \frac{1 + \cos\theta}{2} \quad (59)$$

with $\mu = vk_f$ and the scattering wave vector $q =$

$2k_f \cos \theta/2$. The angular expressions come from the wave-vector dependence of the relative phase of graphene Bloch band wave functions⁶⁸. Since $q < 2k_f$ we have for the polarization⁶⁹ $\Pi(0, q) = -\frac{\partial n}{\partial \mu}$ and for the dielectric function

$$\epsilon(0, q) = 1 - V(q)\Pi(0, q) = 1 + \alpha_V \frac{gk_f}{2q} \quad (60)$$

with the feinstrucure constant of graphene $\alpha_V = e^2/4\pi\epsilon_0\hbar v$ and the degeneracy $g = 4$. The screened Coulomb potential in quasi 2D reads therefore⁶⁹

$$V(q) = \frac{e^2}{2\epsilon_0} \frac{\hbar}{q + \alpha_V \frac{gk_f}{2}}. \quad (61)$$

Using this potential in (59) one gets

$$\frac{\tau\mu}{\hbar} = \frac{8}{\pi g \alpha_V^2} \frac{n}{n_s} c\left(\frac{\alpha_V g}{4}\right) \quad (62)$$

with the constant

$$c(a) = \frac{8}{1 + 2a^2(9 - 60a^2 + 56a^4) + 16a^3(4 - 7a^2)\sqrt{a^2 - 1}}. \quad (63)$$

For the unscreened potential we have $c(0) = 8$ and for the screened one $c(\alpha_V g/4) \approx 74$ such that the relaxation time would be 9 times smaller for unscreened potentials. The relaxation time for the screened potential is also plotted in figure 8. Here we have assumed that the ratio of density to impurities $n/n_s \approx 1/4$ according to valley degeneracy and charge neutrality. It is visible that the unscreened potential is ruled out and the relaxation times agrees with the best-fitted one. If we had used the analytical result (62) directly and fitted only the effective Zeeman field, visibly the same figure 7 would have appeared. This shows that the actual relaxation time from impurity concentration is quite realistic.

In the theoretical approach⁷⁰ it was found that the conductivity is still underestimated even taking into account the effect of optical and acoustic phonons as well as charged impurities and midgap states. We find a slight overestimate when allowing an effective Zeeman field.

To illustrate the relevance of the effective Zeeman field we plot in the next figure 9 the curves with and without Zeeman field. We find a fairly good description of the experimental optical conductivity with a simple relaxation time assuming only charged impurities. The Zeeman field leads to a better agreement of the dissipative part of conductivity with experiments.

The influence of finite-temperatures is marginal as seen in figure 10 while the effective Zeeman field leads to appreciable modifications.

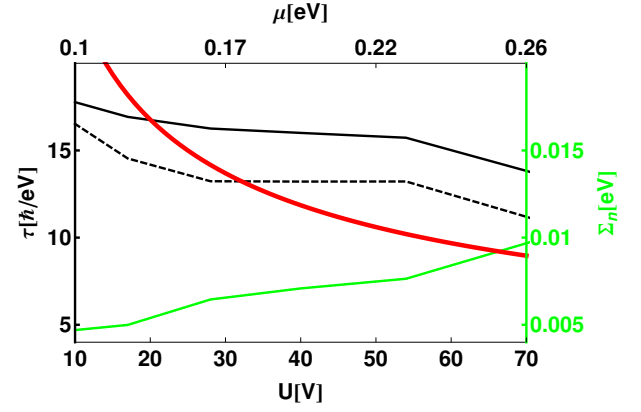


FIG. 8. (Color online) Fitting effective Zeeman field and relaxation time to reproduce the experimental data in figure 7. The best fit only with relaxation time (dashed) is compared to the relaxation time for screened Coulomb impurities (thick black) together with the analytical (red thick) result of (62). The effective Zeeman field (green) is given with the units on the right axis.

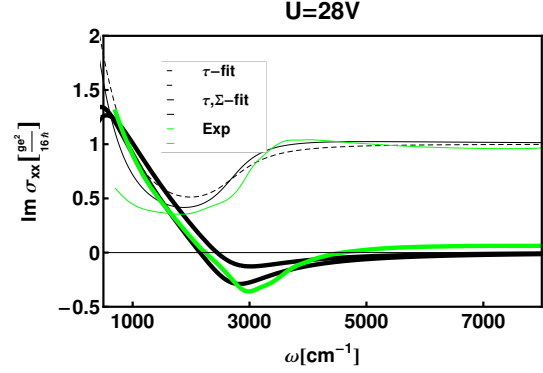


FIG. 9. Comparison of best fit to real (thin) and imaginary (thick) experimental data (green) of figure 7 for $U = 28V$ using once the relaxation time and the effective Zeeman field (solid) and once only the relaxation time (dashed).

B. Hall conductivity

Let us assume the magnetic field in z -direction and the electric field in x -direction. Then we have for graphene

$$\begin{aligned} \sigma_{xy} &= 2e^2 \lambda^2 \frac{\Sigma_n}{v} \mathcal{E} \\ &= \frac{e^2}{2\pi\hbar} \left(\frac{\Sigma_n}{T} \right) \left(\frac{T\tau_\omega}{\hbar} \right)^2 \int_{\frac{\Sigma_n}{T}}^{\infty} dx \frac{\left(e^{\frac{-x-\mu}{T}} + 1 \right)^{-1} - \left(e^{\frac{x-\mu}{T}} + 1 \right)^{-1}}{1 + 4x^2 \left(\frac{T\tau_\omega}{\hbar} \right)^2}. \end{aligned} \quad (64)$$

The Hall conductivity for particles with $p^2/2m$ dispersion at zero temperature and $\mu > \Sigma$ reads¹⁷

$$\sigma_{xy} = \frac{e^2}{4\pi\hbar^2} \Sigma_n \tau_\omega \arctan \left[\frac{4\epsilon_v \tau_\omega / \hbar}{\hbar^2 + 4(2\epsilon_v \mu + \Sigma_n^2) \tau_\omega^2} \right] \quad (65)$$

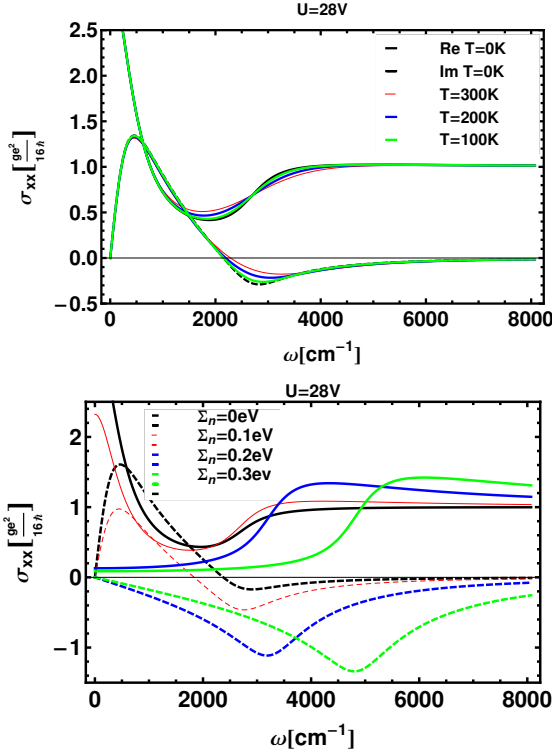


FIG. 10. The influence of finite temperatures (above) and the effective Zeeman field (below).

with the energy $\epsilon_v = mv^2$ and the chemical potential (Fermi energy) μ . The dynamical result is given by the frequency dependence (44) in (65) and (64). We see that the anomalous Hall effect vanishes with vanishing effective Zeeman field (33). Therefore we need an external magnetic field or an effective magnetized domain in order to observe the anomalous Hall effect in graphene.

The infinite-mass limit reads now

$$\sigma_{xy} = \frac{e^2}{4\pi\hbar^2} \tau \omega \Sigma_n \begin{cases} \arccot \frac{2\mu\tau\omega}{\hbar}, & \mu > \Sigma_n \\ \arccot \frac{\Sigma_n\tau\omega}{\hbar}, & \mu < \Sigma_n \end{cases}$$

$$\rightarrow \frac{e^2}{8\pi\hbar} \begin{cases} \frac{\Sigma_n}{\mu} + o(\tau\omega^{-1}), & \mu > \Sigma_n \\ 1 + o(\tau\omega^{-1}), & \mu < \Sigma_n \end{cases} \quad (66)$$

$$\frac{\Sigma_n\tau}{\hbar} \left(\pi - \frac{4\tau\mu}{\hbar} + o(\mu^2) \right), \quad \mu > \Sigma_n$$

which is nothing but the zero-temperature limit of (64). One sees that a step-like structure appears if the chemical potential exceeds the effective magnetic field Σ_n . Remarkably, for larger effective Zeeman field Σ_n we obtain a result independent of the chemical potential and therefore independent on the density. Even in the limit of vanishing scattering the universal value $\sigma_{xy} \rightarrow e^2/8\pi\hbar$ appears.

The temperature dependence of the static Hall conductivity is seen in figure 11. For large effective Zeeman fields the universal limit is approached. The finite-temperature results versus chemical potential are seen in figures 12 which shows the appearance of the threshold at chemical

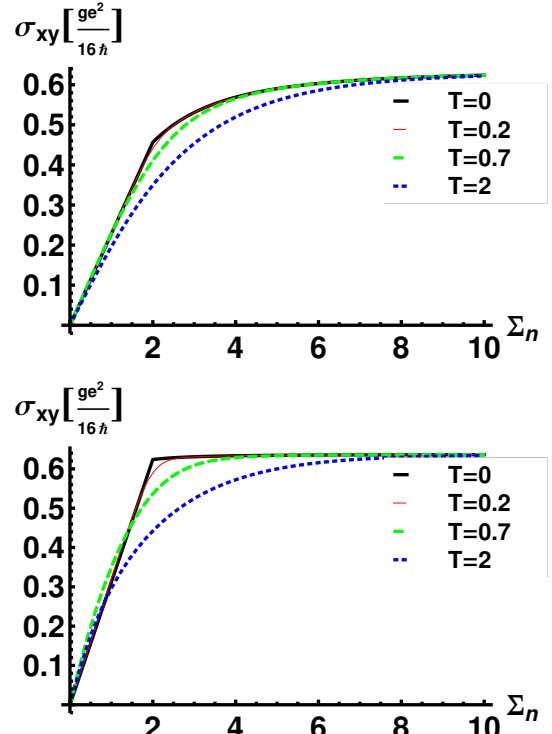


FIG. 11. Temperature dependence (in arbitrary energy units EU) of the static Hall conductivity (64) versus effective Zeeman field with $\mu = 2EU$ for $\tau = 0.2\hbar/EU$ (above) and $\tau = 1\hbar/EU$ (below) where the universal limit in these units is $2/\pi$.

potentials in the order of the Zeeman energy above which the conductivity decreases while below it is constant and determined uniquely by the Zeeman energy.

The dynamical conductivity according to (44) is shown in figure 13. The real part has a sharp maximum at the interband transition frequency where the imaginary part starts. This feature is smeared out by collisions.

C. Expansion in feinstrucutre constant

The different conductivities can be expanded in terms of the graphene feinstrucutre constant α_V . This expansion is also not interchangeable with the small-density expansion. The results are identical with and without screening in lowest order in α_V and read

$$\sigma_{xy} = \frac{ge^2}{16\hbar} \begin{cases} \frac{\Sigma_n}{\mu} \left(\frac{2}{\pi} - \frac{\pi}{96} \frac{n_s}{4n} \alpha_V^4 + o(\alpha_V^6) \right), & \mu > \Sigma_n \\ \frac{2}{\pi} - \frac{\pi\mu^2}{96\Sigma_n^2} \frac{n_s}{4n} \alpha_V^4 + o(\alpha_V^6), & \mu < \Sigma_n \end{cases} \quad (67)$$

The second line appears as well if we first expand up to orders $o(\mu^2)$ which agrees with the universal limit.

For the longitudinal conductivity we obtain

$$\sigma_{xx} = \frac{ge^2}{16\hbar} \begin{cases} \frac{64(\mu^2 - \Sigma_n^2)}{\mu^2\pi^2} \frac{4n}{n_s} \alpha_V^{-2} + o(\alpha_V^0), & \mu > \Sigma_n \\ \frac{\mu}{12\Sigma_n\pi^2} \frac{n_s}{4n} \alpha_V^2 + o(\alpha_V^4), & \mu < \Sigma_n \end{cases} \quad (68)$$

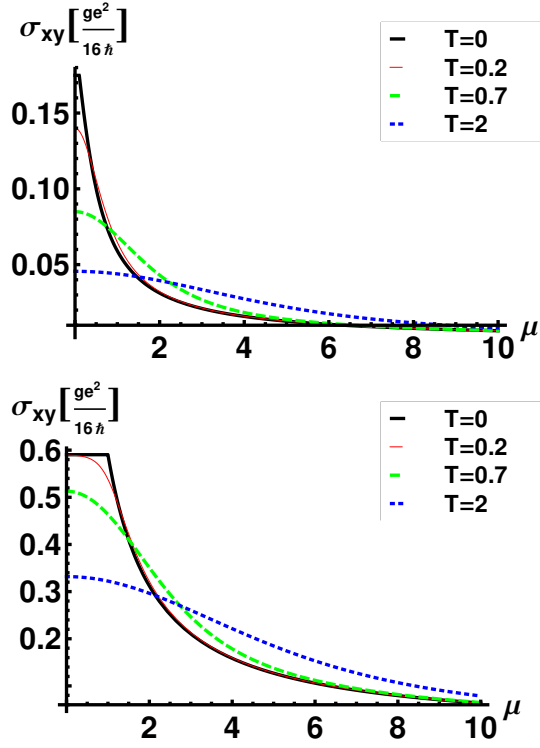


FIG. 12. Temperature dependence (in arbitrary energy units EU) of static Hall conductivity (64) of graphene with $\Sigma_n = 0.1EU$ (above) and $\Sigma_n = 1EU$ (below) and $\tau = 1\hbar/EU$.

which is in contrast to the expansion first in density and then in finestructure constant

$$\sigma_{xx} = \frac{ge^2}{16\hbar} \left(1 + \frac{8162\mu^6}{3n_s^2\pi^7v^6}\alpha_V^{-6} + o(\mu^7) + o(\alpha_V^{-4}) \right) \quad (69)$$

which agrees with the universal limit. One sees completely different expansion schemes depending whether we expand first with respect to the density or with respect to the finestructure constant.

VI. SPIN CONDUCTIVITY

Now we consider the spin current according to (18)

$$\vec{S}_j = 2 \sum_p \left(\partial_j \epsilon \delta \vec{g} + \delta f \partial_{p_j} \vec{b} \right) \quad (70)$$

where the first part is the normal and the second part is the anomaly part. For graphene in the limit of infinite mass we would not expect a normal part since $\partial_j \epsilon = p_j/m \rightarrow 0$ at a first glance. However there is a subtle problem here. In¹⁷ we have calculated this first normal part as

$$\vec{S}_\alpha = -\frac{e\tau}{m_e(1-i\omega\tau)} \vec{s} E_\alpha + \vec{\sigma}_{\alpha\beta} E_\beta. \quad (71)$$

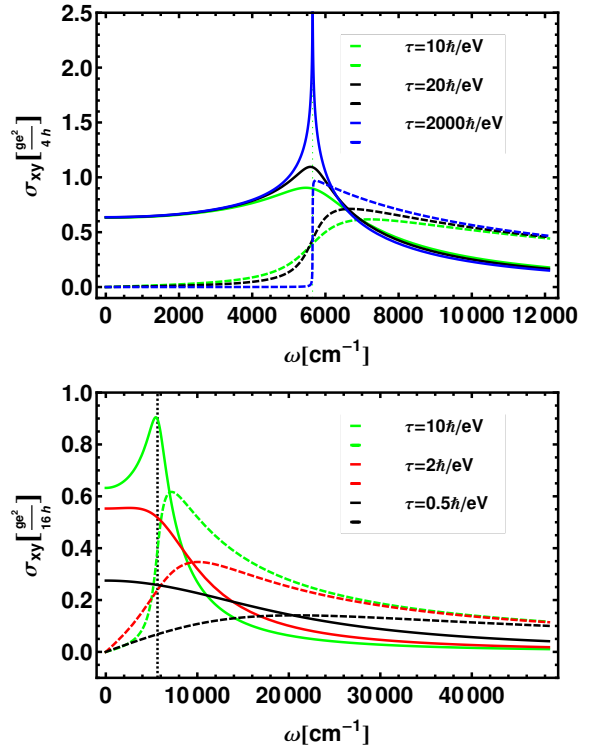


FIG. 13. Dynamical Hall conductivity (66) of graphene with $\Sigma_n = 0.35eV$ and $U = 10V$ for different relaxation times. The dashed vertical line gives the interband transition energy $\max[2\mu, 2\Sigma_n]$

The spin-Hall coefficient consists analogously as the anomalous Hall effect of a symmetric and an asymmetric part ($\omega \rightarrow \omega + i/\tau$)

$$\left. \begin{array}{l} \vec{\sigma}_{\alpha\beta}^{\text{as}} \\ \vec{\sigma}_{\alpha\beta}^{\text{sym}} \end{array} \right\} = \frac{e}{m_e\omega} \sum_p \frac{p_\alpha g}{1 - \frac{\omega^2}{4|\Sigma|^2}} \left\{ \begin{array}{l} \frac{i\omega}{2|\Sigma|} \vec{e} \times \partial_\beta \vec{e} \\ i\partial_\beta \vec{e} \end{array} \right. \quad (72)$$

with the explicit integration in zero temperature and linear Rashba and Dresselhaus coupling¹⁷

$$\begin{aligned} \sigma_{yx}^z &= \frac{e}{8\pi\hbar} \left[1 - \frac{1 + 4\Sigma_n^2\tau_\omega^2}{4\epsilon_\beta\tau_\omega} \arctan\left(\frac{4\hbar\epsilon_\beta\tau_\omega}{\hbar^2 + 4\tau_\omega^2(2\epsilon_\beta\epsilon_F + \Sigma_n^2)} \right) \right] \\ \sigma_{xx}^z &= \frac{2}{\hbar} \Sigma_n \tau \sigma_{yx}^z \end{aligned} \quad (73)$$

with $\tau_\omega = \tau/(1 - i\omega\tau)$. Neglecting the selfenergy and using the static limit it is just the result of^{71,72}.

For graphene we perform the limit of infinite mass of (73). Amazingly we obtain just the universal limit

$$\lim_{m \rightarrow \infty} \sigma_{yx}^z = \frac{e}{8\pi\hbar} \quad (74)$$

contrary to the expectation at the beginning of this chapter that this normal parts of spin current should vanish. This shows a puzzle. The infinite-mass limit of the normal spin-Hall conductivity leads to a finite result though the quasiparticle velocity $\partial_j \epsilon$ vanishes.

The so-called universal limit appears if one takes the limit of vanishing collision frequency

$$\sigma_{yx}^z = \frac{e}{8\pi\hbar} \frac{2\epsilon_\beta\epsilon_f}{2\epsilon_\beta\epsilon_f + \Sigma_n^2} + o(1/\tau). \quad (75)$$

We see how the selfenergy including the Zeeman term (33) modifies this "universal limit" which questions this notion.

For the Dresselhaus linear spin-orbit coupling one has (73) with opposite sign.

The universal constant $e/8\pi\hbar$ has been first described by⁷³ and raised an intensive discussion. It was shown that the vertex corrections cancel this constant^{74,75}. A suppression of Rashba spin-orbit coupling has been obtained due to disorder⁷⁶, or electron-electron interaction⁷⁷ and found to disappear in the self-consistent Born approximation⁷⁸. The conclusion was that the two-dimensional Rashba spin-orbit coupling does not lead to a spin-Hall effect as soon as there are relaxation mechanisms present which damp the spins towards a constant value. In order to include such effects one has to go beyond meanfield and relaxation-time approximation by including vertex corrections⁷⁹. The spin-Hall effect does not vanish with magnetic fields or spin-dependent scattering processes⁷².

Please note that the universal constant in (73) is necessary to obtain the correct small spin-orbit coupling result

$$\sigma_{yx}^z = \frac{e}{\pi\hbar} \frac{\epsilon_f\tau^2}{(1 - i\omega\tau)^2 + 4\Sigma_n^2\tau^2} \epsilon_\beta + o(\epsilon_\beta^2). \quad (76)$$

Without the Zeeman term $\Sigma_n \rightarrow 0$ and for small spin-orbit coupling this agrees with the dynamical result of⁵³ where the definition of spin current has been employed in terms of physical argumentation. Again the result here differs from the resonant structure found in⁵³ by the *arctan* term but the static limit agrees with the result of^{71,72}.

We consider now the anomalous part as the second part of (70). Calculating explicitly for graphene with $\vec{b} = v(p_x, p_y, 0)$ one obtains

$$\vec{S}_j^a = 2 \sum_p \delta f \partial_{p_j} \vec{b} = 2v\delta n \vec{e}_j \quad (77)$$

which shows that the spin current follows the spinor direction. From the mean-field-free response functions (30), as it should be for conductivity, we obtain the density variation

$$\delta n = \frac{v}{\omega} \vec{q} \cdot \delta \vec{s} \quad (78)$$

and using (19) one gets after performing the angular integration

$$\vec{q} \cdot \delta \vec{s} = \vec{q} e \left[-\frac{i}{\omega} (\mathcal{D} + \mathcal{B}) \vec{e}_\alpha + 2 \frac{\Sigma_n}{\omega^2} \mathcal{E} \vec{e}_z \times \vec{e}_\alpha \right] E_\alpha. \quad (79)$$

Using the electric field again in x-direction the anomalous spin current conductivity reads

$$\vec{\sigma}_{jx}^a = \frac{v}{\omega} \vec{e}_j \left[\frac{\sigma_{xx}}{e} q_x + \frac{\sigma_{xy}}{e} q_y \right] \quad (80)$$

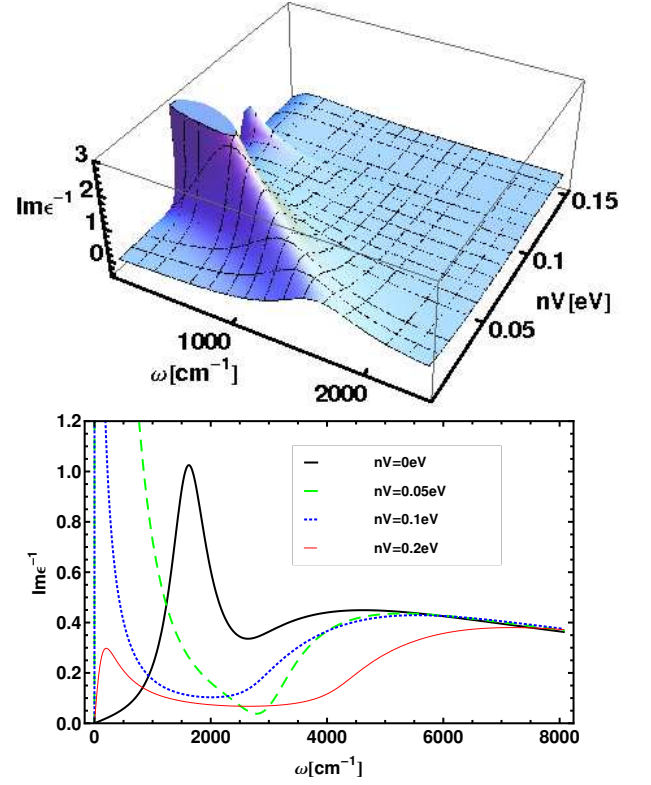


FIG. 14. The excitation function versus frequency and domain interactions as 3D plot (above) and cut at different domains strength (below) for $vq = 1\text{eV}$ and a density corresponding to $28V$ of figure 9.

with the anomalous current conductivities (40) and (64) and the two possible directions $j = x, y$ providing spin-Hall and spin conductivity. We see that the anomaly spin conductivity is wavelength dependent and vanishes in the long-wavelength limit.

VII. DIELECTRIC FUNCTION

The induced density is related to the external potential by the response function $\delta n = \chi \Phi$. The screened potential V^s is given by the external potential Φ and the interacting one V_0 by $V^s = V_0 \delta n + \Phi$. The ratio of the screened to the external potential is the inverse dielectric function

$$\frac{1}{\epsilon} = \frac{V^s}{\Phi_{\text{ext}}} = 1 + V_0 \chi. \quad (81)$$

In other words, the electrons feel the effective potential V_0/ϵ . Though the Coulomb interaction is repulsive a change in sign of the dielectric function indicates an effective attraction as it is the mechanism for Cooper pairing due to phonon coupling. It is interesting to search for such regions as possible range where Cooper pairing can occur in graphene.

The response can be calculated straightforwardly from the linear equation system (30). The result is a lengthy expression. Only special expansions are needed here. In the optical regime the coupling velocity v of graphene is about $1/300$ of the speed of light and one has the small parameter

$$\eta = \frac{vq}{\hbar\omega} = \frac{1}{300}. \quad (82)$$

Expanding the response function one obtains in the optical regime

$$\frac{1}{\epsilon} = 1 - \frac{\omega}{\omega} \eta^2 - i \frac{\omega^2}{\omega^2 \bar{\sigma}} \frac{\pi\alpha}{16} \eta^3 + o(\eta^4) \quad (83)$$

with the dimensionless conductivity $\bar{\sigma} = 16\hbar\sigma_{xx}/ge^2$ from (40) and the feinstrucure constant $\alpha \approx 1/137$. We see that the deviation of the inverse dielectric function in the optical regime is only in orders of 10^{-4} and cannot lead to any sign change.

This is different if we consider the non-optical regime, where $\hbar\omega \neq cq$. Then η is no small parameter anymore and we can only expand with respect to the feinstrucure constant leading to

$$\epsilon = 1 + i \frac{\bar{\sigma}}{1 + \frac{2\Sigma_n V v^2 q^2}{\omega \hbar^4 \bar{\omega}^3 \omega} \mathcal{F}} \frac{\pi\alpha}{16} + o(\alpha^2) \quad (84)$$

where \mathcal{F} from (34) reads for $T = 0$

$$\mathcal{F} = -\frac{\Theta(\mu - \Sigma_n)}{4\pi\hbar^2 v^2} \frac{\mu^2 - \Sigma_n^2}{1 + 4\tau_n^2 \mu^2}. \quad (85)$$

The collective modes are visible at places where the real part becomes zero and a small imaginary part of ϵ representing the damping. This is best visualized by the excitation function $-\text{Im}\epsilon^{-1}$ as plotted in figures 14. We see that with increasing magnetic domain strength V the collective peak becomes sharpened and shifted towards lower frequencies. The second peak around $V = 0.1$ is at the line $\mu \leq \Sigma_n$ where \mathcal{F} vanishes. In⁴² negative excitations indicating spin-separation instabilities have been found for certain polarizations. Here in graphene no such regions are observed.

In the next figure 15 we plot the contours of the excitation functions indicating the small damping together with the area where the real part of the dielectric function changes sign. We see that the lower part of the collective excitation is accompanied by a negative area. Since this comes together with small damping, i.e. with a small imaginary part of ϵ , we can consider this range as the one where the repulsive interaction changes effectively into attractive interaction and pairing is possible.

This range of attractive interaction is dependent on the wave vector and the magnetic domain meanfield as illustrated in the next figure 16. The magnetic domain allows this sign change at smaller wavelengths though the frequency range shrinks with increasing magnetic domain strength. The here reported sign change is a prerequisite for Cooper pairing. A detailed analysis of the possibility to have superfluidity and superconductivity in graphene can be found in⁸⁰⁻⁸².

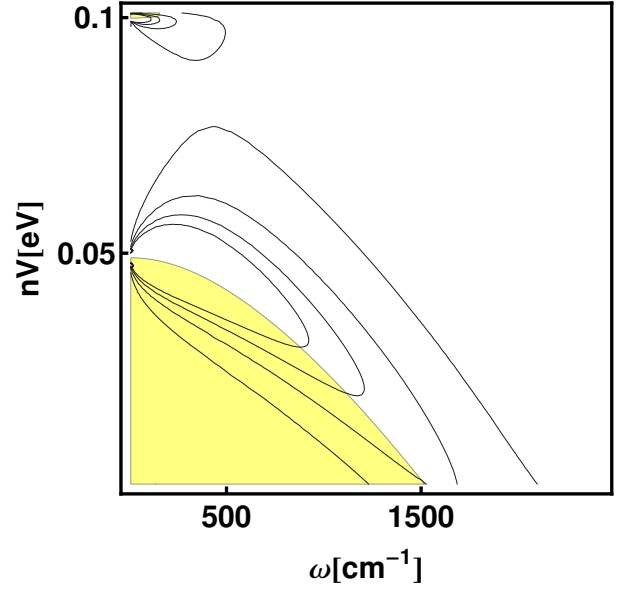


FIG. 15. The contour lines of figure 14 together with the range where the real part of dielectric function becomes negative (yellow).

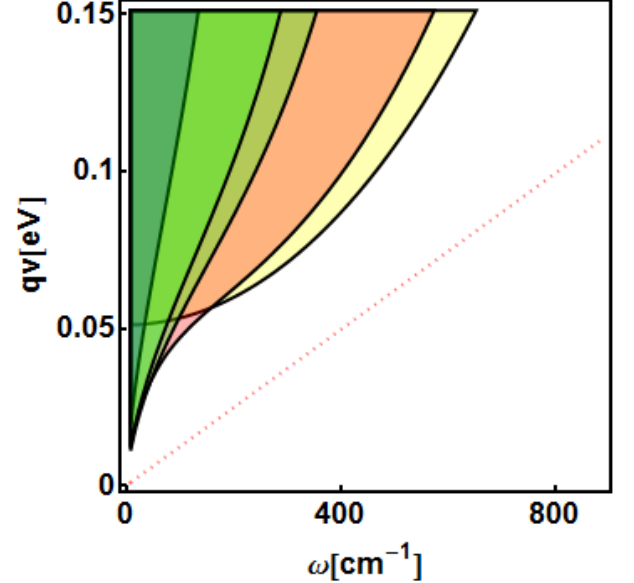


FIG. 16. The range of sign change of interaction potential for different magnetic domain meanfields; from left to right: $nV = 0, 0.02, 0.06, 0.07, 0.09$ eV. The straight line illustrates $\hbar\omega = qv$.

VIII. SUMMARY

The quantum kinetic equations for systems with $SU(2)$ symmetry have been employed to describe the coupling between the Wigner distributions for charge and for spin polarization. The used many-body approximation is on the level of random phase approximation (RPA). This comes about by linearizing the exact meanfield ki-

netic equation and using the relaxation time for screened Coulomb interaction.

Using the results from electrons with quadratic mass dispersion and spin-orbit coupling, one can obtain the linear Dirac dispersion of electrons in graphene by the infinite-mass limit. This allows to translate many results obtained for spin-polarized systems with spin-orbit coupling to graphene. We discuss here the density and spin currents. For the density currents no quasiparticle part appears only anomalous ones. The anomalous currents lead to intra- and interband longitudinal conductivities and the Hall conductivity.

We have analyzed the conductivities with respect to the influence of magnetic fields and magnetic domain puddles as well as meanfields which can be recast into an effective Zeeman field. A density-independent universal behavior appears for large Zeeman fields or for small densities. The experimental optical conductivity is well reproduced by an intrinsic effective Zeeman field and a proper relaxation time calculated in RPA. Various limits are found not to be interchangeable like the limit of vanishing scattering and the static limit. Only the systematic expansion with respect to vanishing density leads to the universal value. The spin current shows a subtlety in that the infinite-mass limit leads non-trivially to

a universal value for the quasiparticle part though the quasiparticle velocity vanishes.

The dynamical density and spin response functions are derived as coupled linear equations system. By linearization of the exact meanfield kinetic equations for density and spin, the response in random phase approximation (RPA) with relaxation time-approximation is obtained. Though the standard RPA-Lindhard polarization function vanishes for graphene, the anomalous coupling to the spin-polarization induces different forms of polarization functions which are presented explicitly. The resulting dielectric function is discussed with respect to the expansion in orders of the finestructure constant. It is found that the effective Zeeman field is enhancing and sharpening the collective mode until some critical value. This is accompanied with a frequency and wavelength range where the screened interaction changes the sign allowing the electrons to form Cooper pairs. Though the used level of RPA should be extended to better approximations in order to achieve quantitative predictions for pairing, the qualitative region is believed to maintain. Finally we should emphasize that we have considered all quantities up to fourth order in wavelength expansion which can be overcome by mean-field-free approximations of the polarization function⁴⁹.

-
- ¹ A. H. Castro Neto, F. Guinea, N. M. R. Peres, K. S. Novoselov, and A. K. Geim, *Rev. Mod. Phys.* **81**, 109 (2009).
 - ² D. S. L. Abergel, V. Alpakov, J. Berashevich, K. Ziegler, and T. Chakraborty, *Adv. Phys.* **59**, 261 (2010).
 - ³ S. Das Sarma, S. Adam, E. H. Hwang, and E. Rossi, *Rev. Mod. Phys.* **83**, 407 (2011).
 - ⁴ H. C. Kao, M. Lewkowicz, and B. Rosenstein, *Phys. Rev. B* **82**, 035406 (2010).
 - ⁵ A. W. W. Ludwig, M. P. A. Fisher, R. Shankar, and G. Grinstein, *Phys. Rev. B* **50**, 7526 (1994).
 - ⁶ K. S. Novoselov, A. K. Geim, S. V. Morozov, D. Jiang, M. I. Katsnelson, I. V. Grigorieva, S. V. Dubonos, and A. A. Firsov, *Nature* **438**, 197 (2005).
 - ⁷ R. R. Nair, P. Blake, A. N. Grigorenko, K. S. Novoselov, T. J. Booth, T. Stauber, N. M. R. Peres, and A. K. Geim, *Science* **320**, 1308 (2008).
 - ⁸ A. B. Kuzmenko, E. van Heumen, F. Carbone, and D. van der Marel, *Phys. Rev. Lett.* **100**, 117401 (2008).
 - ⁹ Y.-W. Tan, Y. Zhang, K. Bolotin, Y. Zhao, S. Adam, E. H. Hwang, S. Das Sarma, H. L. Stormer, and P. Kim, *Phys. Rev. Lett.* **99**, 246803 (2007).
 - ¹⁰ E. H. Hwang, S. Adam, and S. D. Sarma, *Phys. Rev. Lett.* **98**, 186806 (2007).
 - ¹¹ K. Ziegler, *Phys. Rev. Lett.* **97**, 266802 (2006).
 - ¹² K. Ziegler, *Phys. Rev. B* **75**, 233407 (2007).
 - ¹³ J. Cserti, *Phys. Rev. B* **75**, 033405 (2007).
 - ¹⁴ J. Kailasvuori, B. Sopik, and M. Trushin, *Journal of Statistical Mechanics: Theory and Experiment* **2013**, P12006 (2013).
 - ¹⁵ D. Culcer and R. Winkler, *Phys. Rev. B* **78**, 235417 (2008).
 - ¹⁶ D. Culcer, E. H. Hwang, T. D. Stanescu, and S. Das Sarma, *Phys. Rev. B* **82**, 155457 (2010).
 - ¹⁷ K. Morawetz, *Phys. Rev. B* **92**, 245425 (2015), errata: *Phys. Rev. B* **93** (2016) 239904(E).
 - ¹⁸ T. Louvet, P. Delplace, A. A. Fedorenko, and D. Carpentier, *Phys. Rev. B* **92**, 155116 (2015).
 - ¹⁹ M. I. Katsnelson, *Eur. Phys. J. B* **51**, 157 (2006).
 - ²⁰ W. Yi-Xiang, H. Yue-Juan, and X. Shi-Jie, *Modern Physics Letters B* **26**, 1 (2012).
 - ²¹ W. S. Bao, S. Y. Liu, X. L. Lei, and C. M. Wang, *Journal of Physics: Condensed Matter* **21**, 305302 (2009).
 - ²² G. Dávid, P. Rakya, L. Oroszlány, and J. Cserti, *Phys. Rev. B* **85**, 041402 (2012).
 - ²³ S. Teber and A. V. Kotikov, *EPL (Europhysics Letters)* **107**, 57001 (2014).
 - ²⁴ B. Rosenstein, M. Lewkowicz, and T. Maniv, *Phys. Rev. Lett.* **110**, 066602 (2013).
 - ²⁵ I. F. Herbut, V. Juričić, and O. Vafek, *Phys. Rev. Lett.* **100**, 046403 (2008).
 - ²⁶ E. G. Mishchenko, *Europ. Phys. Lett.* **83**, 17005 (2008).
 - ²⁷ D. E. Sheehy and J. Schmalian, *Phys. Rev. B* **80**, 193411 (2009).
 - ²⁸ G. Gazzola, A. L. Cherchiglia, L. A. Cabral, M. C. Nemes, and M. Sampaio, *Europ. Phys. Lett.* **104**, 27002 (2013).
 - ²⁹ V. Juričić, O. Vafek, and I. F. Herbut, *Phys. Rev. B* **82**, 235402 (2010).
 - ³⁰ I. Sodemann and M. M. Fogler, *Phys. Rev. B* **86**, 115408 (2012).
 - ³¹ A. C. Ferrari and e. al., *Nanoscale* **7**, 4598 (2015).
 - ³² M. I. Katsnelson and A. K. Geim, *Phil. Trans. R. Soc. A* **366**, 195 (2008).
 - ³³ R. Reiter, U. Derra, S. Birner, B. Terrés, F. Libisch, J. Burgdörfer, and C. Stampfer,

- Phys. Rev. B **89**, 115406 (2014).
- ³⁴ Z. Chen and X.-Q. Wang, Phys. Rev. B **83**, 081405 (2011).
 - ³⁵ N. M. R. Peres, F. Guinea, and A. H. Castro Neto, Phys. Rev. B **73**, 125411 (2006).
 - ³⁶ W. Wang and A. H. Jayatissa, Synthetic Metals **204**, 141 (2015).
 - ³⁷ A. Ljam, R. Saidur, P. Ganesan, and A. M. Golsheikh, Int. J. Heat and Mass Trans. **87**, 92 (2015).
 - ³⁸ Y. Zhang, V. W. Brar, C. Girit, A. Zettl, and M. F. Crommie, Nature Physics **5**, 722 (2009).
 - ³⁹ Q. Li, E. H. Hwang, and S. Das Sarma, Phys. Rev. B **84**, 115442 (2011).
 - ⁴⁰ R. Bao and L. Moriconi, Physics Letters A **379**, 1492 (2015).
 - ⁴¹ J. Chen and S. Hershfield, Phys. Rev. B **57**, 1097 (1998).
 - ⁴² K. Morawetz, Phys. Rev. B **92**, 245426 (2015).
 - ⁴³ C. L. Kane and E. J. Mele, Phys. Rev. Lett. **95**, 226801 (2005).
 - ⁴⁴ Z. Qiao, S. A. Yang, W. Feng, W.-K. Tse, J. Ding, Y. Yao, J. Wang, and Q. Niu, Phys. Rev. B **82**, 161414 (2010).
 - ⁴⁵ W.-K. Tse, Z. Qiao, Y. Yao, A. H. MacDonald, and Q. Niu, Phys. Rev. B **83**, 155447 (2011).
 - ⁴⁶ G. Tkachov, Phys. Rev. B **79**, 045429 (2009).
 - ⁴⁷ N. Mermin, Phys. Rev. B **1**, 2362 (1970).
 - ⁴⁸ K. Morawetz, Phys. Rev. E **88**, 022148 (2013).
 - ⁴⁹ G. L. Klimchitskaya and V. M. Mostepanenko, Phys. Rev. B **93**, 245419 (2016).
 - ⁵⁰ U. Briskot, M. Schütt, I. V. Gornyi, M. Titov, B. N. Narozhny, and A. D. Mirlin, Phys. Rev. B **92**, 115426 (2015).
 - ⁵¹ M. Auslender and M. I. Katsnelson, Phys. Rev. B **76**, 235425 (2007).
 - ⁵² B. E. Sernelius, Journal of Physics: Condensed Matter **27**, 214017 (2015).
 - ⁵³ V. V. Bryksin and P. Kleinert, Phys. Rev. B **73**, 165313 (2006).
 - ⁵⁴ J.-I. Inoue, G. E. W. Bauer, and L. W. Molenkamp, Phys. Rev. B **67**, 033104 (2003).
 - ⁵⁵ L. A. Falkovsky and A. A. Varlamov, Europ. Phys. J B **56**, 281 (2007).
 - ⁵⁶ J. Z. Bernád, M. Jääskeläinen, and U. Zülicke, Phys. Rev. B **81**, 073403 (2010).
 - ⁵⁷ J. Z. Bernád, U. Zülicke, and K. Ziegler, Physica E: Low-dimensional Systems and Nanostructures **42**, 755(2010).
 - ⁵⁸ S. Xiao, X. Zhu, B.-H. Li, and N. A. Mortensen, Front. Phys. **11**, 117801 (2016).
 - ⁵⁹ T. Ando, Y. Zheng, and H. Suzuura, J. Phys. Soc. Japan **71**, 1318 (2002).
 - ⁶⁰ B. Wunsch, T. Stauber, F. Sols, and F. Guinea, New J. of Phys. **8**, 318 (2006).
 - ⁶¹ T. Fukuzawa, M. Koshino, and T. Ando, J. Phys. Soc. Japan **78**, 094714 (2009).
 - ⁶² D. Yudin, O. Eriksson, and M. I. Katsnelson, Phys. Rev. B **91**, 075419 (2015).
 - ⁶³ A. Hill, A. Sinner, and K. Ziegler, Eur. Phys. J. B **86**, 53 (2013).
 - ⁶⁴ P. R. Wallace, Phys. Rev. **71**, 622 (1947).
 - ⁶⁵ T. Stauber, N. M. R. Peres, and A. K. Geim, Phys. Rev. B **78**, 085432 (2008).
 - ⁶⁶ Y. Zhang, Y.-W. Tan, H. L. Stormer, and P. Kim, Nature **438**, 201 (2005).
 - ⁶⁷ Z. Q. Li, E. A. Henriksen, Z. Jiang, Z. Hao, M. C. Martin, P. Kim, H. L. Stormer, and D. N. Basov, Nature Physics **4**, 532 (2008).
 - ⁶⁸ K. Nomura and A. H. MacDonald, Phys. Rev. Lett. **96**, 256602 (2006).
 - ⁶⁹ K. Morawetz, Phys. Rev. B **67**, 115125 (2003).
 - ⁷⁰ T. Stauber, N. M. R. Peres, and A. H. Castro Neto, Phys. Rev. B **78**, 085418 (2008).
 - ⁷¹ J. Schliemann and D. Loss, Phys. Rev. B **69**, 165315 (2004).
 - ⁷² J. Schliemann, Int. J. of Mod. Phys. B **20**, 1015 (2006).
 - ⁷³ J. Sinova, D. Culcer, Q. Niu, N. A. Sinitsyn, T. Jungwirth, and A. H. MacDonald, Phys. Rev. Lett. **92**, 126603 (2004).
 - ⁷⁴ J.-I. Inoue, G. E. W. Bauer, and L. W. Molenkamp, Phys. Rev. B **70**, 041303 (2004).
 - ⁷⁵ R. Raimondi and P. Schwab, Phys. Rev. B **71**, 033311 (2005).
 - ⁷⁶ O. Chalaev and D. Loss, Phys. Rev. B **71**, 245318 (2005).
 - ⁷⁷ O. V. Dimitrova, Phys. Rev. B **71**, 245327 (2005).
 - ⁷⁸ S. Y. Liu, X. L. Lei, and N. J. M. Horing, Phys. Rev. B **73**, 035323 (2006).
 - ⁷⁹ G. Zala, B. N. Narozhny, and I. L. Aleiner, Phys. Rev. B **64**, 214204 (2001).
 - ⁸⁰ Y. E. Lozovik, S. L. Ogarkov, and A. A. Sokolik, Phys. Rev. B **86**, 045429 (2012).
 - ⁸¹ F. Guinea and B. Uchoa, Phys. Rev. B **86**, 134521 (2012).
 - ⁸² K. V. Germash and D. V. Fil, Phys. Rev. B **93**, 205436 (2016).